文章编号：1001－9014(2018)06－0673－06

DOI:10.11972/j.issn.1001－9014.2018.06.006

25-channel 200 GHz AWG based on SOI ridge waveguides

YUAN Pei[1,2], WANG Yue[1,*], WU Yuan-Da[1,2,*], LIU Li-Jie[1,2], An Jun-Ming[1,2], HU Xiong-Wei[1]

(1. State Key Laboratory of Integrated Optoelectronics, Institute of Semiconductors, Chinese Academy of Science, Beijing 100083, China;
2. College of Materials Science and Opto-Electronic Technology, University of Chinese Academy of Sciences, Beijing 100049, China)

Abstract: A SOI-based 25-channel AWG with 200 GHz channel spacing is demonstrated. The minimum distance between the input waveguides (Δx_i)/ output waveguides (Δx_o)/ arrayed waveguides (d) is optimized respectively. Then the boundary structures between the free propagation regions (FPRs) and the arrayed waveguides (W_2/L_2/L_3) are optimized in detail. The experiment results show that the insertion loss of the AWG is 5 ~ 7 dB, and the crosstalk of it is 13 ~ 15 dB. Compared with our previous work, the performance of AWG in this paper has been improved greatly, and further methods to improve the performances of insertion loss and crosstalk have been proposed as well.

Key words: silicon photonics, arrayed waveguide gratings, double-etch structure, wavelength division multiplexing/de-multiplexer

PACS: 42.79.Gn, 42.79.Sz, 42.82.Et

基于绝缘体上硅材料的25通道200 GHz的阵列波导光栅

袁　配[1,2]，王　玥[1,*]，吴远大[1,2,*]，刘丽杰[1,2]，安俊明[1,2]，胡雄伟[1]

(1. 中国科学院半导体研究所 集成光电子学国家重点实验室,北京　100083;
2. 中国科学院大学 材料科学与光电技术学院,北京　100049)

摘要:报道了基于绝缘体上硅材料的25通道、信道间隔200 GHz的阵列波导光栅,分别优化了输入波导/输出波导/阵列波导间的最小间距(Δx_i/Δx_o/d),及其自由传播区和阵列波导之间边界结构(W_2/L_2/L_3).实验结果表明,该阵列波导光栅的插入损耗为5～7 dB,串扰为13～15 dB,该阵列波导光栅的性能得到有效提升.同时也提出了减小插损与串扰的进一步优化方案.

关　键　词:硅基光电子;阵列波导光栅;双刻蚀结构;波分复用/解复用器

中图分类号:TN256　　**文献标识码**:A

Introduction

Silicon photonics[1-3] has been the hot topic in optical communication system recently. With high refractive contrast, silicon on insulator (SOI) waveguides allow small bent radius, small footprint and therefore high-level integration of many optical functions[4-11] on a single chip. Besides, silicon photonics is compatible with the mature complementary metal oxide semiconductor (CMOS) technology. Based on these advantages, the production cost of optical communication devices and systems can be greatly cut down, showing that silicon photonics is a promising solution for future high-speed optical interconnections.

Arrayed waveguide grating (AWG)[12-18] based on SOI is a key component in wavelength division multiplexing (WDM) system. High confined silicon AWG allows great reduction in footprint compared to tradition low-contrast waveguide platforms. However, high refractive contrast results in small tolerance in fabrication process. For example, small side wall roughness will greatly increase insertion loss; small fabrication non-uniformity in the silicon layer thickness and mask layer will introduce large phase error and thus increasing the crosstalk and wavelength shift. Therefore, the reported performances of

Received date: 2018-03-26, **revised date**: 2018-08-24　　**收稿日期**:2018-03-26, **修回日期**:2018-08-24

Foundation items: Supported by National Key R&D Program of China (2016YFB0402504)

Biography: YUAN Pei(1989-), female, Baoding, China, Ph. D student, Mainly engaged in the research of SOI based tunable optical waveguide devices. E-mail: yuanpei@semi.ac.cn

* **Corresponding author**: E-mail: wy1022@semi.ac.cn, wuyuanda@semi.ac.cn

SOI-based AWGs such as crosstalk, insertion loss, loss uniformity and flap top are not all that satisfactory.

Methods have been proposed either by improving the fabrication process or by optimizing the designs to improve the performances of AWGs. In this paper, a 25-channel 200 GHz AWG based on SOI platform with 220 nm-thick top silicon layer has been fabricated and two ways have been taken to stabilize the performance of the AWGs. One is to widen the width of arrayed waveguides, and the other is to adopt the double-etch structure at the boundary between the free propagation regions and the arrayed waveguides.

1 Design and fabrication

1.1 device structure and principle

A typical AWG is composed of input/output waveguides, input/output free propagation region (FPR) and arrayed waveguides, as shown in Fig. 1.

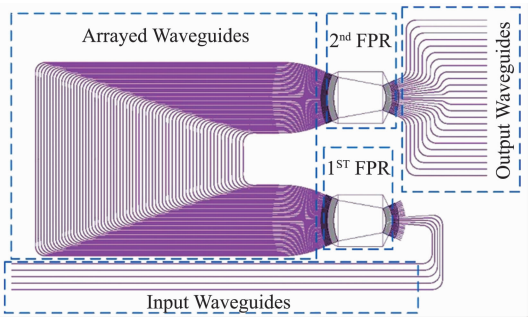


Fig. 1 The structural diagram of an AWG
图 1 阵列波导光栅的结构示意图

Multi-wavelength optical signals from one of the input waveguides (always the central one) will diverge at the input free propagation region (1st FPR), and then the divergent light with the same phase information will couple to the arrayed waveguides. Because of the fixed length difference between the adjacent arrayed waveguides, the optical signal transmitting through the adjacent arrayed waveguides have the same phase difference, which will interfere with each other at the output free propagation region (2nd FPR). Various wavelength channels will be focused in different spatial position. As a result, different optical signals with different wavelength will be output by the output waveguides. Throughout the process, the light propagation meets the grating diffraction equation:

$$n_s(\lambda)d\sin\theta_i + n_s(\lambda)d\sin\theta_o + n_c(\lambda)\Delta L = m\lambda \quad ,(1)$$

where n_s/n_c is the refractive index of the slab waveguide at FPRs; λ is the wavelength of optical signal; d is the minimum separation distance between the adjacent arrayed waveguides; θ_i/θ_o is the diffraction angels at the input/output slabs; ΔL is the length difference between the adjacent arrayed waveguides; m is the diffraction order.

1.2 Simulation and optimization

A rib waveguide is adopted in this paper. To ensure the single mode condition, the width and the etching depth of the waveguide is 500 nm and 150 nm, respectively.

First of all, the minimum distances between the input waveguides (Δx_i)/output waveguides (Δx_o)/arrayed waveguides (d) must be determined to ensure that there is no crosstalk caused by the mutual coupling between two waveguides. Figure 2 shows the corresponding simulated results. Both Figs. 2 (a) and (b) show the contour map of electric field (E_y) and the relationship between the monitored output optical power of both waveguides and time (c is the velocity of light in vacuum, and T represents time) when the distance between the two straight waveguides (D) is 0.6 μm and 1 μm, respectively. From Fig. 2 (a) and (b) it can be seen that there is obvious coupling between the two waveguides when the distance between them is 0.6 μm, while there is hardly any coupling when the distance is changed to 1 μm. Figure 2 (c) is the dependence of the normalized output optical power on the distance between the two waveguides. Obviously, the output optical power of Wg. 1 increases and that of Wg. 2 decreases as the two waveguides stay further, and then basically remains unchanged when the distance is larger than 1 μm for both waveguides. So, it can be concluded that if the distance between two straight waveguides is larger than 1 μm, the coupling between them can be neglected. As a result, the minimum distance between adjacent arrayed waveguides (d) is designed to be 1 μm, and the minimum distance between adjacent input/output waveguides (Δx_i/ Δx_o) is set to be 1.5 μm. The parameters of AWG calculated according to the diffraction equation is listed in Table 1.

Table 1 The designed parameters of the AWG
表 1 AWG 的设计参数

Parameter	Value
Thickness of top silicon of SOI (H)	220 nm
Waveguides width (w)	500 nm
Thickness of slab waveguides (h)	70 nm
Central wavelength (λ_0)	1.52 μm
Channel spacing ($\Delta\lambda$)	1.6 nm
Number of input/output channels (N_i/ N_o)	5/25
Pitch width of arrayed waveguide (d)	1 μm
Pitch width of input/output waveguides ($\Delta x_i/\Delta x_o$)	1.5 μm
Radius of Rowland circle (R)	82.13 μm

Since the effective-refractive-index (n_{eff}) related optical performance of silicon AWG such as crosstalk is severely sensitive to the fabrication tolerance and non-uniformity as described in the introduction section, methods must be taken to reduce the impact of fabrication non-uniformity.

Figure 3 shows the dependence of the effective refractive index of a waveguide on its width under different etching depth (H_{etch}), from which it can be seen that the width fluctuation has a smaller impact on the n_{eff} of the waveguide with a wider rib. Obviously it is preferable to take a wider waveguide because for wider waveguide. The fabrication non-uniformity of its width has a smaller impact on its effective refractive index and then the crosstalk of AWG may be impacted lightly. However, there may be some disadvantages to take wider waveguides, one of which is that the bending loss of wi-

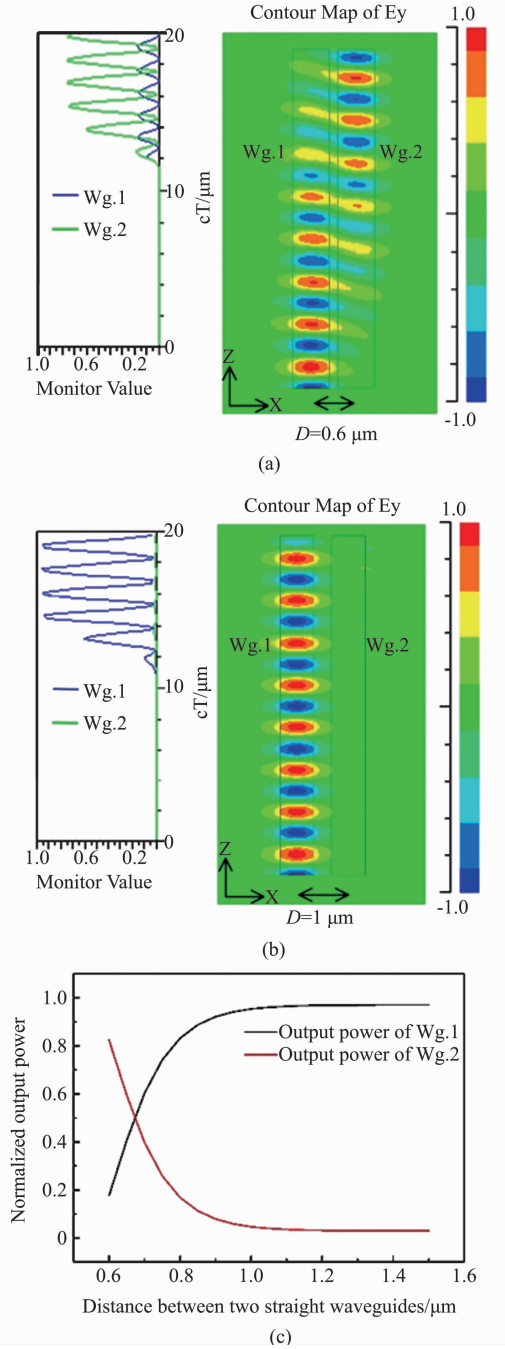


Fig. 2　Simulation of the minimum distances between input/output/arrayed waveguides (a) The optical field distribution (D = 0.6 μm), (b) the optical field distribution (D = 1 μm), (c) the dependence of the normalized output power on the distance of the two straight waveguides

图 2　输入/输出/阵列波导的最小间距的模拟 (a) 波导间距为 0.6 μm 时的光场分布,(b) 波导间距为 1 μm 时的光场分布,(c) 两直波导的归一化输出光功率随其间距的变化关系

der waveguides may become larger because high-order modes will generate in wider waveguides and the minimum bent radius of high order modes is larger than that of the fundamental modes. In conclusion, in order to reduce the phase error caused by the fabrication non-uniformity, the waveguides in the straight section of arrayed waveguides are widened from 500 nm to 800 nm and in order to reduce the insertion loss and avoid mode mixing inside the 800 nm wide waveguides, the width of bend waveguides remains 500 nm[17], as shown in Fig. 4.

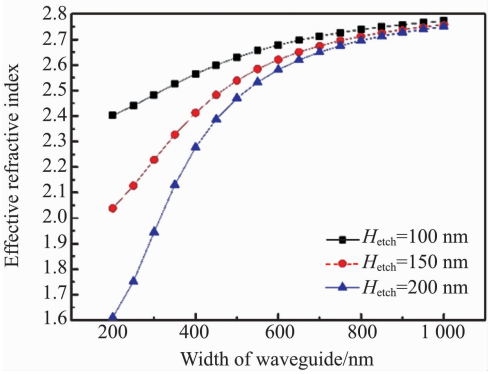


Fig. 3　Simulated effective refractive index of waveguide with different widths and etching depths

图 3　波导有效折射率随波导宽度和刻蚀深度的变化关系

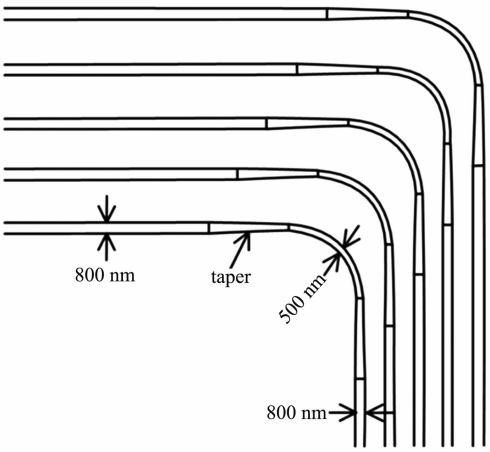


Fig. 4　The diagram of widened arrayed waveguides

图 4　阵列波导展宽结构示意图

The insertion loss of an AWG consists of the propagation loss, bending loss, the transition loss between FPRs and arrayed/input/output waveguides, and the transition loss accounts for the key part of the insertion loss. So the boundary structures between the FPRs and the arrayed/input/output waveguides must be optimized to decrease the insertion loss. In this paper, tapers and double-etch structures are used to reduce the insertion loss.

The double-etch structure is shown in Fig. 5, which contains 3 stages. The first stage is a rib waveguide structure with 70nm-slab thickness (h), the third stage is a rib waveguide structure with 150 nm-slab thickness (h_3), and the second stage is a double-rib structure transiting from the first stage to the third stage. The parameters that need to be determined are the final width of the 2nd rib on the 2nd stage (W_2), the length (L_2) of the 2nd stage, and the length of the taper on the 3rd stage

(L_3) which connects the 2nd stage and the FPRs.

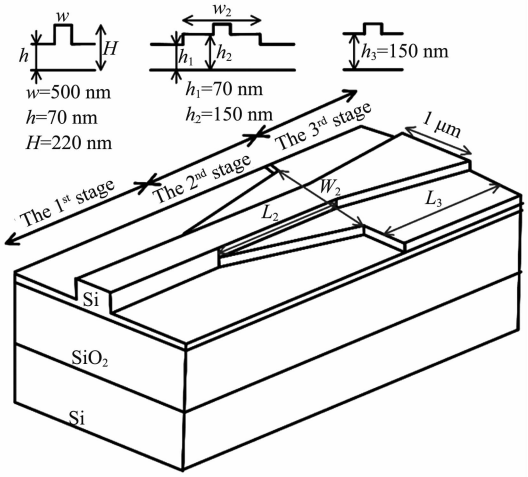


Fig. 5 The diagram of the double-etch structure
图5 双刻蚀结构示意图

First of all, the final width of the 2nd rib on the second stage can be obtained from Fig. 6, which is how the effective refractive index of the double - rib waveguide changes with the final width of the 2nd rib on the second stage (W_2). It can be seen that the effective index increases with W_2 being larger, and when W_2 is larger than 1.5 μm, the curve of Fig. 6 basically becomes flat and remains unchanged. As a result, the parameter W_2 is assigned to be 1.7 μm to realize the perfect transition from the 1st stage to the 3rd stage without sudden change of the refractive index. That means there is no sudden change of mode field and thus decreasing the insertion loss.

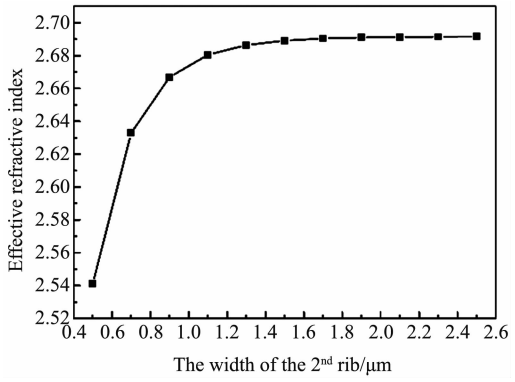


Fig. 6 The dependence of the effective refractive index of the double-rib waveguide on the width of the 2nd rib (W_2)
图6 双脊波导的有效折射率随其第二脊宽度的变化关系

On the other hand, the length of the 2nd stage (L_2) also needs to be determined. 3D-FDTD method is used to simulate the transmission of the 2nd stage as a function of the length of it, as is shown in Fig. 7. From Fig. 7 it can be seen that the output optical power increases gradually when increasing the length of the 2nd stage and will stays stable when the 2nd stage is longer than 4 μm. This means the perfect transition between two different modes will be realized and the loss caused by mode mismatch between the two modes is negligible when the length of the 2nd stage is longer than 4 μm. In this paper, the length of the 2nd stage is selected to be 10 μm.

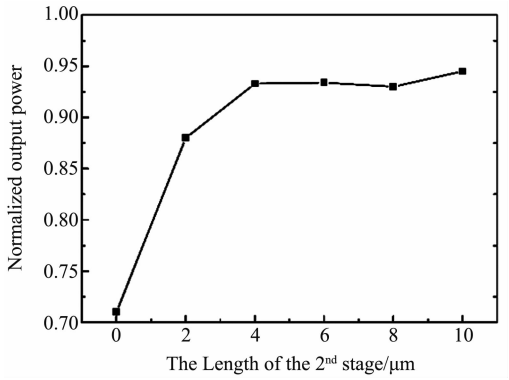


Fig. 7 The dependence of the Normalized output power on the length of the double-rib waveguide on the 2nd stage
图7 归一化输出光功率随第二阶段双脊波导长度的变化关系

At last, the transmission of the taper on the 3rd stage as a function of the length of it (L_3) is simulated as shown in Fig. 8. From Fig. 8 it can be seen that the normalized output power of the taper on the 3rd stage raises as the length of it (L_3) increases, and when L_3 is larger than 3 μm, the output power stays unchanged basically. This is because longer taper makes slower mode conversion from large spot size to a small one, and then the loss caused by mode mismatch will decrease. When L_3 is larger than 3 μm, the taper is long enough to realize a perfect transition between two different modes. In this paper, the length of the taper on the 3rd stage is designed to be 10 μm.

1.3 Device fabrication

The fabrication processes are as follows. First of all, the waveguide pattern is transferred to the wafer by deep ultraviolet lithography (DUVL) technology, and then silicon waveguides with etching depth of 150nm are fabricated using the inductively coupled plasm (ICP) technology. Later, DUVL and ICP technology are both used to form the waveguides with etching depth of 70

Table 2 Comparisons with our previous work
表2 与前期工作的对比

Reference	The number of channels	Channel spacing	$\Delta x_i/\Delta x_o/d$	Minimum insertion loss	Crosstalk
Ref. [19]	16	200 GHz	2.25/2.25/2.25 μm	6 dB	7.5 dB
This paper	25	200 GHz	1.5/1.5/1 μm	5 dB	13 ~ 15 dB

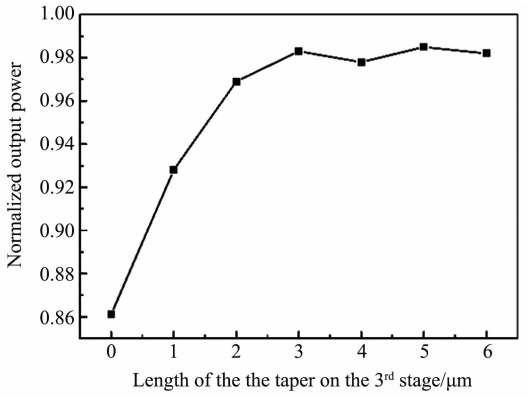


Fig. 8　The dependence of the Normalized output power on the length of the taper on the 3rd stage
图 8　归一化输出光功率随第三阶段锥形波导的变化关系

nm. Finally, a 1.25 μm-thick SiO_2 protecting layer is grown by plasma enhanced chemical vapor deposition (PECVD) technology to protect the AWG. The fabricated chip of the 25-channel AWG is shown in Fig. 9.

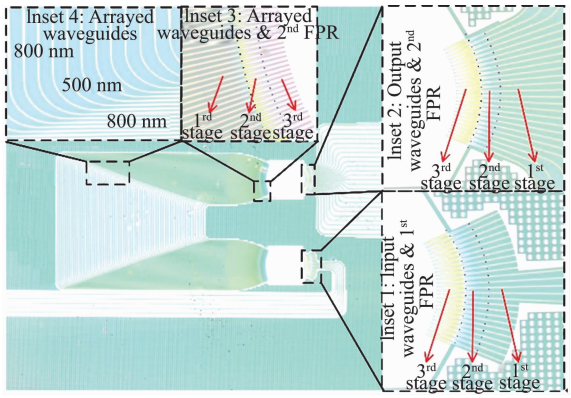


Fig. 9　The micrograph of the fabricated 25-channel AWG
图 9　25 通道阵列波导光栅的显微图片

2　Characterization and discussion

The tested spectrum of the AWG is shown in Fig. 10, from which it can be seen that the insertion loss of the AWG is 5 ~ 7 dB. The factors that contribute this include the loss of bent waveguides, the loss caused by the side-wall roughness, and the loss caused by the mode mismatch between the FPRs and the input/output/arrayed waveguides. As mentioned earlier, double-etch structures and tapers have been adopted to reduce the loss generated at the boundary between the FPRs and the input/output/arrayed waveguides, and the radius of the bent waveguides is also large enough so that the bending loss is negligible. So it can be concluded the fabrication process needs to be optimized to reduce the side-wall roughness and the boundary between the FPRs and the input/output/arrayed waveguides may need further optimization. The tested results also show that the crosstalk of the AWG is 13 ~ 15 dB. The reasons to cause such high crosstalk may be the fabrication process and the tapers on the 3rd stage. As is mentioned earlier, the crosstalk, which is the result of beam defocusing at the output waveguides due to unequal phase shifts of arrayed waveguides, is very sensitive to fabrication non-uniformity. Widened arrayed waveguides have been taken already, and other ways such as the optimization of the fabrication process must be taken to decrease the fabrication non-uniformity. On the other hand, the simulated optimal length of the taper on the 3rd stage is 3 μm, while the fabricated length is 10 μm, which will also introduce extra crosstalk because the interactive distance of optical signals in different waveguides grows longer. So the length of the tapers on the 3rd stage should be a little shorter to achieve a better performance.

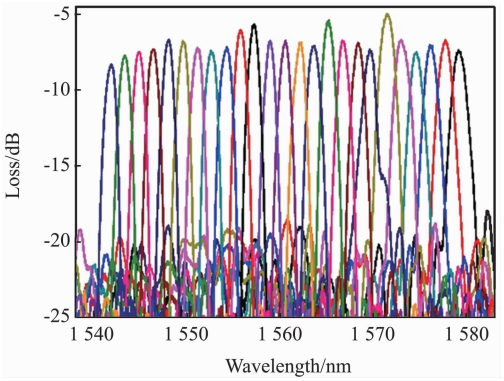


Fig. 10　The tested spectrum of the fabricated AWG
图 10　制作的阵列波导光栅测试图谱

Compared with our previous work[19] which only takes widened arrayed waveguides, the performances of AWG in this paper with both widened arrayed waveguides and double-etch structures have been improved greatly. The performances of both AWGs have been listed in Table 2, from which it can be concluded that by further optimizing the key parameters like $\Delta x_i/\Delta x_o/d$ (the minimum distance between the input waveguides/output waveguides/arrayed waveguides) and $W_2/L_2/L_3$ (the detailed boundary structure parameters between the FPRs and the arrayed waveguides), the insertion loss and crosstalk of AWG can be improved.

3　Conclusion

In this paper, a 25-channel AWG with 200 GHz channel spacing is demonstrated. The optical transmission of two straight waveguides with different waveguide distance (D) is simulated to determine parameters including the minimum distance between the input waveguides (Δx_i)/ output waveguides ($/\Delta x_o$)/arrayed waveguides (d). Then the arrayed waveguides are widened from 500 nm to 800 nm in order to get a high fabrication tolerance. At last the boundary structures between the free propagation regions (FPRs) and the arrayed waveguides are optimized in detail in order to get a boundary structure with low loss. The experiment results show that the insertion loss of the AWG is 5 ~ 7 dB, and the crosstalk of it is 13 ~ 15 dB. Compared with our previous work, the per-

formance of AWG in this paper has been improved greatly, and further methods to improve the performances of insertion loss and crosstalk have both been proposed.

References

[1] Cheng B, Li C, Liu Z, *et al*. Research progress of Si-based germanium materials and devices [J]. J. Semicond., 2016, **37**(8): 081001.

[2] Feilchenfeld N B, Nummy K, Barwicz T, *et al*. Silicon photonics and challenges for fabrication [C]. Proceedings of SPIE. 2017, **10149**: 101490D.

[3] Zhou Z, Wang X, Yi H, *et al*. Silicon photonics for advanced optical communication systems. [J]. *Proceedings of SPIE*. 2013, **8630**: 863014.

[4] Ren B, Hou Y, Liang Y. Research progress of Ⅲ-Ⅴ laser bonding to Si [J]. *J. Semicond.*, 2016, **37**(12): 124001.

[5] Song B, Stagarescu C, Ristic S, et al. 3D integrated hybrid silicon laser [J]. Opt. Exp., 2016, **24**(10): 10435 - 10444 .

[6] Xiao J-B, Li W L, Xia S S, *et al*. Full-vectorial analysis of the directional couplers in vertical multiple-slotted silicon wires with trapezoidal cross-section [J]. *Journal of infrared and millimeter waves*. 2012, **31**(5): 437 - 440.

[7] Spott A, Peters J, Davenport M L, *et al*. Quantum cascade laser on silicon [J]. *Optica*, 2016, **3**(5), 545 - 551.

[8] Wu W, Cheng B, Zhang J, *et al*. High gain-bandwidth product Ge/Si tunneling avalanche photodiode with high-frequency tunneling effect [J]. *J. Semicond.*, 2017, **38**(11): 114003.

[9] Shin M J, Ban Y, Yu B M, *et al*. Parametric characterization of self-heating in depletion-type Si micro-ring modulators [J]. *IEEE Journal of selected topics in quantum electronics*. 2016, **22**(6): 3400207.

[10] Wang Z, Gao Y L, Kashi A S, *et al*. Silicon microring modulator for dispersion uncompensated transmission applications [J]. *Journal of Lightwave Technology*., 2016, **34**(16), 3675 - 3681.

[11] Zhao Z, Liu J, Liu Y, *et al*. High-speed photodetectors in optical communication system [J]. *J. Semicond.*, 2017, **38**(12): 121001.

[12] Fang Q, Li F, Liu Y L. Fabrication of arrayed waveguide grating based on SOI material [J]. *Journal of infrared and millimeter waves*. 2005, **24**(2): 143 - 146.

[13] Ye T, Fu Y, Qiao L, *et al*. Low-crosstalk Si arrayed waveguide grating with parabolic tapers [J]. *Opt. Exp.*, 2014, **22**(26): 31899 - 31906.

[14] Park J, Joo J, Park H, *et al*. Improved performance of a silicon arrayed waveguide grating by reduction of higher order mode generation near the boundary of a star coupler [J]. *Proceeding of SPIE*. 2015, **9367**: 936705.

[15] Li H, Bai Y, Dong X, *et al*. Practical fabrication and analysis of an optimized compact eight-channel silicon arrayed-waveguide grating [J]. *Optical Engineering*. 2013, **52**(6): 064602.

[16] Kim D J, Lee J M, Song J H, *et al*. Crosstalk reduction in a shallow-etched silicon nanowire AWG [J]. *IEEE Photonics Technology Letters*. 2008, **20**(19): 1615 - 1617.

[17] Pathak S, Vanslembrouck M, Dumon P, *et al*. Compact SOI-based polarization diversity wavelength de-multiplexer circuit using two symmetric AWGs [J]. *Opt. Exp.*, 2012, **20**(26): B493 - B500.

[18] Adar R, Henry C H, Dragone C, *et al*. Broad-band array multiplexers made with silica waceguides on silicon [J]. *J. Lightwave Technol.*, 1993, **11**(2): 212 - 219.

[19] Yuan P, Wang Y, Wu Y, *et al*. Design and fabrication of wavelength tunable AWGs based on the thermo-optic effect [J]. *Chin. Opt. Lett.*, 2018, **16**(1): 010601.